



RESEARCH LETTER

10.1002/2013GL059065

Key Points:

- Nordic Seas sea level is largely mass related and coherent with Arctic sea level
- Nonseasonal sea level variability is related to northeast Atlantic winds
- Zonal wind drives northward Ekman transport and impacts Arctic sea level

Correspondence to:

D. L. Volkov,
Denis.Volkov@noaa.gov

Citation:

Volkov, D. L. (2014), Do the North Atlantic winds drive the nonseasonal variability of the Arctic Ocean sea level?, *Geophys. Res. Lett.*, 41, 2041–2047, doi:10.1002/2013GL059065.

Received 17 DEC 2013

Accepted 16 FEB 2014

Accepted article online 24 FEB 2014

Published online 17 MAR 2014

Do the North Atlantic winds drive the nonseasonal variability of the Arctic Ocean sea level?

Denis L. Volkov^{1,2}

¹Cooperative Institute for Marine and Atmospheric Studies, University of Miami, Miami, Florida, USA, ²NOAA, Atlantic Oceanographic and Meteorological Laboratory, Miami, Florida, USA

Abstract The Gravity Recovery and Climate Experiment (GRACE) satellites have observed coherent and nearly uniform nonseasonal fluctuations of bottom pressure throughout the Arctic Ocean and the Nordic Seas. Strong correlation between the nonseasonal GRACE and satellite altimetry data is found in the Nordic and Barents Seas, which suggests a possibility of using the longer altimetry records in these areas as a proxy for the nonseasonal sea level variability over the entire Arctic. This study identifies the dominant pattern of the nonseasonal atmospheric pressure variability that drives strong zonal wind anomalies over the northeastern North Atlantic associated with the nonseasonal sea level anomalies in the Nordic Seas. Our results show that wind-driven northward Ekman transport anomalies in the northeastern North Atlantic may induce coherent changes of sea level across the entire Arctic Ocean.

1. Introduction

Since the advent of satellite altimetry, the monitoring of sea level has become nearly global. However, the presence of sea ice severely limits the observational capabilities of space-borne altimeters in polar regions. Despite some progress in recovering sea surface height (SSH) measurements over open leads in ice-covered Arctic regions [Peacock and Laxon, 2004; Kwok and Morison, 2011], continuous, basin-wide monitoring of the Arctic Ocean SSH is still problematic. Only the monthly ocean mass (Ocm) variations have been continuously observed over the entire Arctic since the launch of the Gravity Recovery and Climate Experiment (GRACE) satellite mission in March 2002 [Tapley et al., 2004]. Numerical models suggest that the variability of the Arctic Ocean SSH is largely mass related, especially over the continental shelf [e.g., Vinogradova et al., 2007; Volkov and Landerer, 2013].

Previous studies have demonstrated the reliability of GRACE observations of the Arctic Ocm changes [e.g., Morison et al., 2007; Peralta-Ferriz and Morison, 2010; Volkov et al., 2013]. Ponte et al. [2007] and later Peralta-Ferriz and Morison [2010] studied the annual cycle of the Arctic Ocm and explained it by freshwater fluxes. Using bottom pressure measurements at the North Pole and in the Beaufort Sea, Peralta-Ferriz et al. [2011] analyzed fast submonthly oscillations of the Arctic Ocm and linked them to the meridional winds over the Nordic Seas that modulate wind-driven slope currents. Disregarding the Ocm variability in the Nordic Seas, Peralta-Ferriz et al. [2014] concluded that the basin-coherent Arctic Ocm responds to inflow mainly through the Fram Strait via a northward Ekman slope current. However, Volkov and Landerer [2013] demonstrated that the area of the basin-coherent Ocm variability includes the Nordic Seas. They showed that the nonseasonal Arctic Ocm variability is mostly driven by the net flow across the boundary between the Nordic Seas and northeast Atlantic at about 65°N. This means that the existing explanation of the Arctic Ocm variability by winds affecting currents only in the Nordic Seas is not complete and that external forcing, south of 65°N in the Atlantic, should be relevant.

The main objective of this study is to understand whether wind forcing over the northeastern North Atlantic can drive the variability of SSH and Ocm in the Nordic Seas and to discuss possible mechanisms. The study will demonstrate that the large-scale nonseasonal SSH variability in the Nordic Seas is mostly mass related. It will also address the question of whether the large-scale nonseasonal SSH variability in the Nordic Seas can be used as a proxy for the large-scale nonseasonal Ocm variability over the entire Arctic Ocean. The latter is important, because continuous satellite altimetry records are limited to ice free areas of the Nordic and Barents Seas, but they are 2 times longer compared to GRACE observations. Therefore, altimetry measurements, when coupled to atmospheric forcing, can provide statistically more robust results.

2. Data and Methods

This study uses the monthly averaged data and focuses on the nonseasonal time scales, i.e., synoptic fluctuations with periods from 2 to 6 months and interannual changes.

2.1. Ocean Mass From GRACE

This study uses the most recent GRACE Release-05 monthly OcM anomalies from January 2003 to December 2012 based on spherical harmonics from the University of Texas Center for Space Research (CSR RL5.0). Details on data processing can be found in *Chambers and Bonin* [2012]. The OcM data are smoothed with a Gaussian filter with 500 km half width. The global mean OcM was subtracted from each time step in order to remove the global atmospheric pressure effect and any net OcM change due to the net global freshwater fluxes. Furthermore, an OcM monthly mean climatology and a linear trend, calculated over the 2003–2012 time interval, were subtracted to focus on the nonseasonal time scales.

2.2. Sea Surface Height From Altimetry

The SSH maps from January 1993 to December 2012 are generated by merging multisatellite altimetry data (Topex/Poseidon, ERS-1/2, Jason-1/2, and Envisat) [*Le Traon et al.*, 1998]. Although the SSH data above 66°N are based on either ERS-1/2 (operational in 1991–2003) or Envisat (operational in 2002–2012), the convergence of ground tracks at high latitudes provides sufficient spatial and temporal coverage to adequately resolve the synoptic-scale variability in the Nordic and Barents Seas [*Volkov and Pujol*, 2012]. The SSH data were used over the 40°N–80°N and 50°W–50°E domain, where sea ice is present only near Greenland and in the Barents Sea. For consistency with GRACE data, the SSH data were monthly averaged and smoothed with a Gaussian filter with 500 km half width. A global average SSH and a monthly mean climatology over the 2003–2012 time interval were subtracted from each time step to remove the effect of global warming and the (predominantly steric in nature) seasonal cycle of SSH.

2.3. Atmospheric Reanalysis Data

Satellite altimetry and GRACE observations were coupled to monthly mean sea level pressure (SLP) and 10 m wind speed data, obtained from the ERA-Interim reanalysis (www.ecmwf.int) [*Dee et al.*, 2011]. A global mean SLP was subtracted from each SLP field and a monthly mean climatology over the 2003–2012 time interval was removed from both the SLP and the wind speed data.

2.4. Methods

An empirical orthogonal functions (EOF) analysis [*von Storch and Zwiers*, 1999] was used to identify the leading mode of the OcM variability over the polar domain north of 60°N, including the Nordic Seas. This mode is characterized by a spatial pattern (Figure 1a) and its temporal evolution, illustrated by the principal component (PC-1) time series (Figure 1b, gray curve). The spatial pattern is represented as a regression map obtained by projecting the OcM data onto the standardized (divided by standard deviation) PC-1 time series. Thus, the regression coefficients are in centimeters (local change in OcM) per standard deviation change in PC-1 of OcM.

A coupled EOF (cEOF) analysis was applied over the 50°W–50°E and 40°N–80°N domain to identify the temporally covarying spatial patterns of SSH (Figure 2a) and SLP (Figure 2b) that explain most of the covariance between the two fields [*Bretherton et al.*, 1992]. The temporal evolution of these patterns is demonstrated by two coupled PC (cPC) time series for SSH and SLP (Figure 3). The cEOF analysis was conducted for both the nonseasonal and low-pass filtered (with a yearly running mean) fields. Only the first cEOF modes (cEOF-1) are considered in this study. The spatial patterns of cEOF-1 are presented in the form of homogeneous correlation maps, i.e., correlation between the cPC-1 time series of SSH/SLP and the SSH/SLP fields (Figures 2a and 2b). The squared correlation coefficients show the portion of the local variance explained by each mode. The monthly nonseasonal SSH and SLP time series from January 1993 to December 2012 have 240 records. Accounting for the autocorrelation of the time series (especially SSH), the number of effective degrees of freedom is about 20. This means that correlation coefficients above 0.4 are significant at the 95% confidence level.

Regression analysis is then used to examine the structure of wind anomalies associated with the cEOF-1 mode of the SLP variability: the zonal and meridional ERA-Interim 10 m wind speed data are projected onto the standardized cPC-1 time series of SLP to obtain regression maps of wind vectors (Figure 2c). The

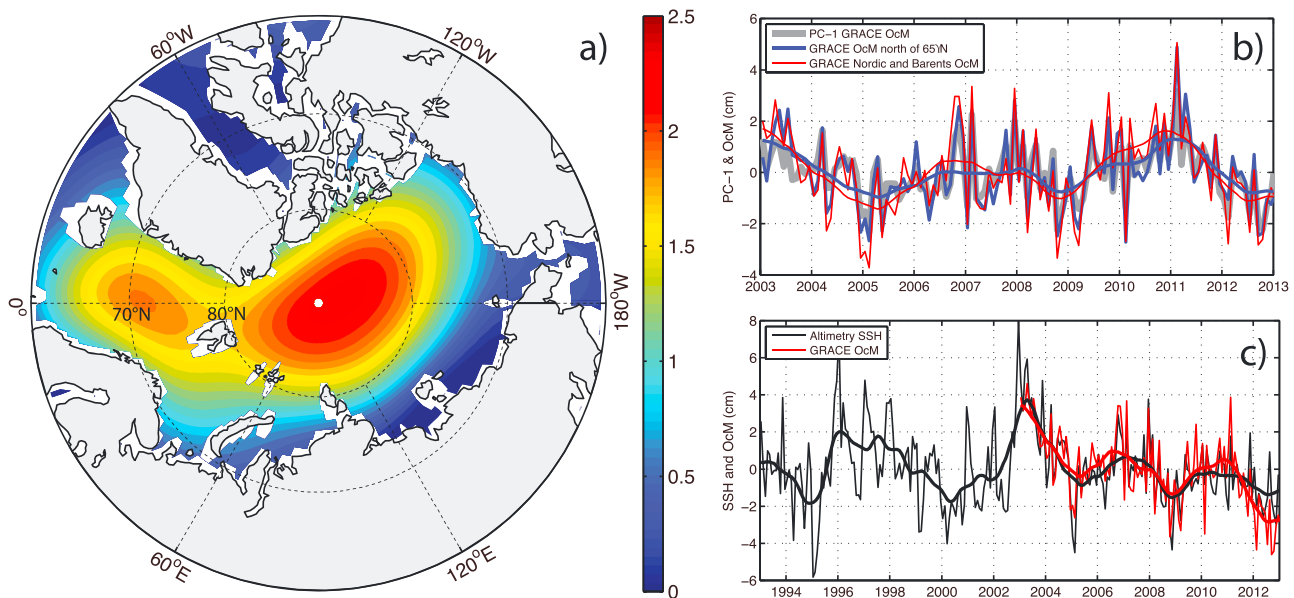


Figure 1. (a) The EOF-1 of the nonseasonal OcM shown as a regression map (cm/standard deviation) obtained by projecting the OcM data onto the standardized (divided by standard deviation) PC-1 time series. (b) The PC-1 of the nonseasonal OcM (gray curve) and the detrended nonseasonal OcM averaged over the entire Arctic domain (north of 65°N, blue curve) and over the Nordic and Barents Seas (red curve). (c) The nonseasonal SSH (black curve) and OcM (red curve) averaged over the Nordic and Barents Seas. The interannual changes are shown by yearly running means.

corresponding regression coefficients are in m s^{-1} (local change in wind speed) per standard deviation change in cPC-1 of SLP.

3. Results

3.1. Basin-Coherent Changes of Sea Level

The EOF-1 mode of the GRACE OcM explains 68.2% of the OcM variance and exhibits an almost uniform spatial pattern that extends over the deep parts of the Arctic Ocean and over the Nordic Seas south to about 60°–65°N (Figure 1a). The maximum magnitude of coherent OcM changes is about 2 cm/standard deviation, with the magnitude near the North Pole being slightly larger than in the Nordic Seas. The temporal evolution of EOF-1 and the time series of OcM, averaged over the entire Arctic domain (north of 65°N) and over the Nordic and Barents Seas (40°E–50°W and 65°N–80°N) are strongly correlated with each other (Figure 1b). The zero-lag correlation coefficients are 0.91 between PC-1 and the Arctic OcM, 0.89 between PC-1 and the Nordic and Barents OcM, and 0.92 between the Arctic OcM and the Nordic and Barents OcM. The time series demonstrate that the OcM variability in the Arctic Ocean and in the Nordic and Barents Seas is characterized by coherent nonseasonal signals, including interannual. GRACE observed two full cycles with a period of about 4 years over the 2003–2012 time interval. Due to the observed coherency in the basin-wide nonseasonal OcM fluctuations, it is reasonable to assume that at the time scales considered the OcM variability in the Nordic and Barents Seas is representative of the OcM variability over most of the Arctic Ocean.

The Nordic and Barents Seas have been well monitored by altimetry satellites for over two decades [Volkov and Pujol, 2012]. Displayed in Figure 1c are the time series of the nonseasonal SSH anomalies from 1993 to 2012 (black curves) and OcM anomalies from 2003 to 2012 (red curves), averaged over 40°E–50°W and 65°N–80°N. An important prerequisite for this study is a strong correlation between the concurrent monthly altimetry and the GRACE data after the removal of the monthly mean climatology (no linear trend removed). The zero-lag correlation coefficients are 0.80 between the nonseasonal time series and 0.88 between their yearly running means. The record maximum SSH occurred in winter 2002/2003. The variability of SSH was stronger prior to 2003 with a standard deviation of 2.6 cm, while the standard deviation of SSH after 2003 was 2.1 cm. The interannual variability of SSH manifests periodicities of about 5 years in 1995–2005 and about 4 years in 2005–2012.

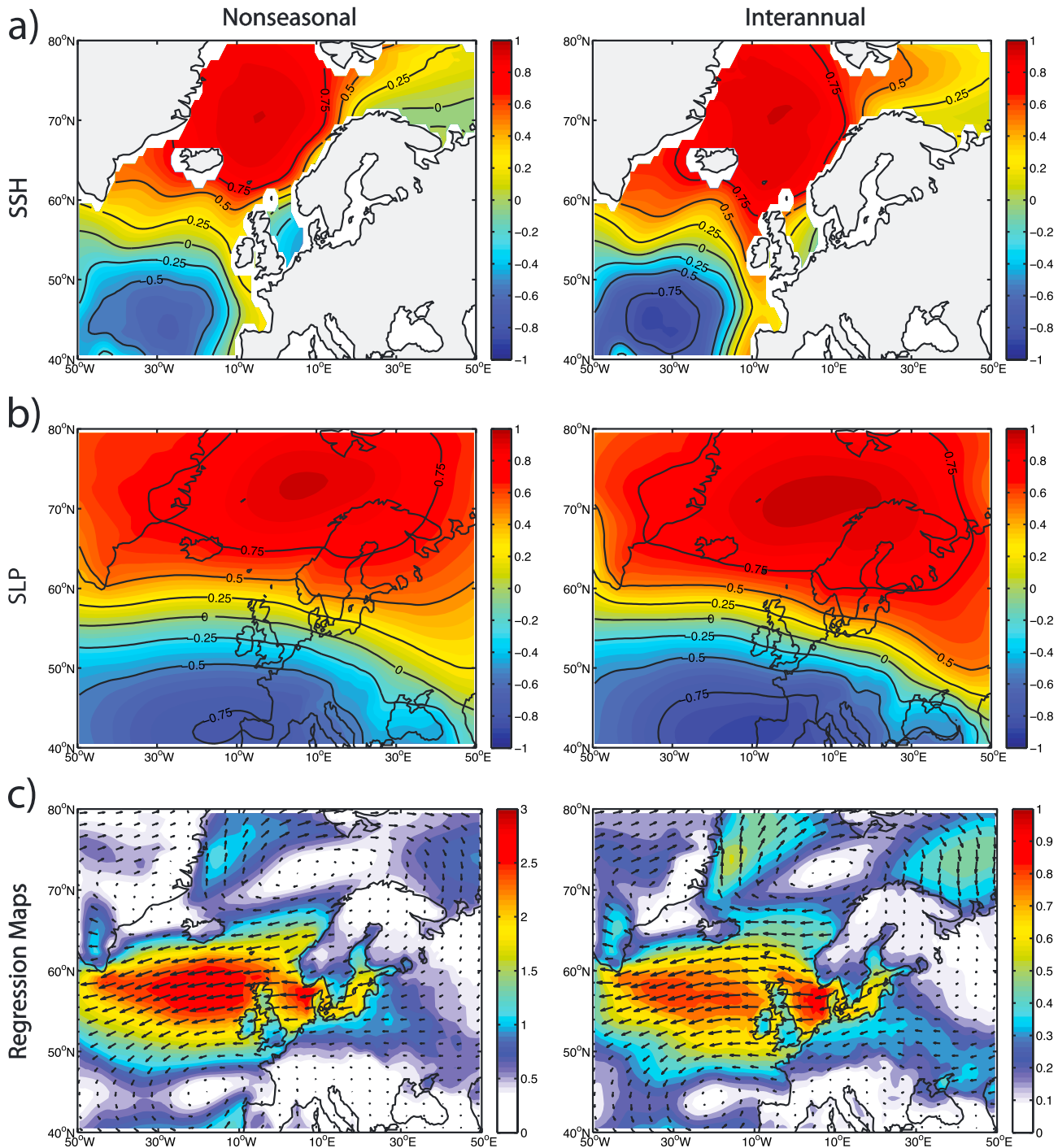


Figure 2. The cEOF-1 spatial patterns shown as homogeneous correlation maps: (a) correlation between the cPC-1 of SSH (black curves in Figure 3) and the SSH data and (b) correlation between the cPC-1 of SLP (red curves in Figure 3) and the SLP data; (c) the regression maps of the ERA-Interim winds projected on cPC-1 of SLP fields. Units in Figure 2c are in m s^{-1} per standard deviation. Figures 2a–2c show the results obtained for the nonseasonal/interannual SSH, SLP, and wind velocity fields.

These observations indicate that the large-scale nonseasonal SSH variability over the Nordic and Barents Seas in 2003–2012 was mostly mass related. It is reasonable to extrapolate this relationship to the entire Arctic Ocean domain and to the entire observational period from 1993 to 2012. It appears that the local steric variability is effectively removed by subtracting the monthly mean climatology. Because the global mean SSH was subtracted from each time step, it means that the nonseasonal steric variability due to local warming is practically inseparable from the global warming effect.

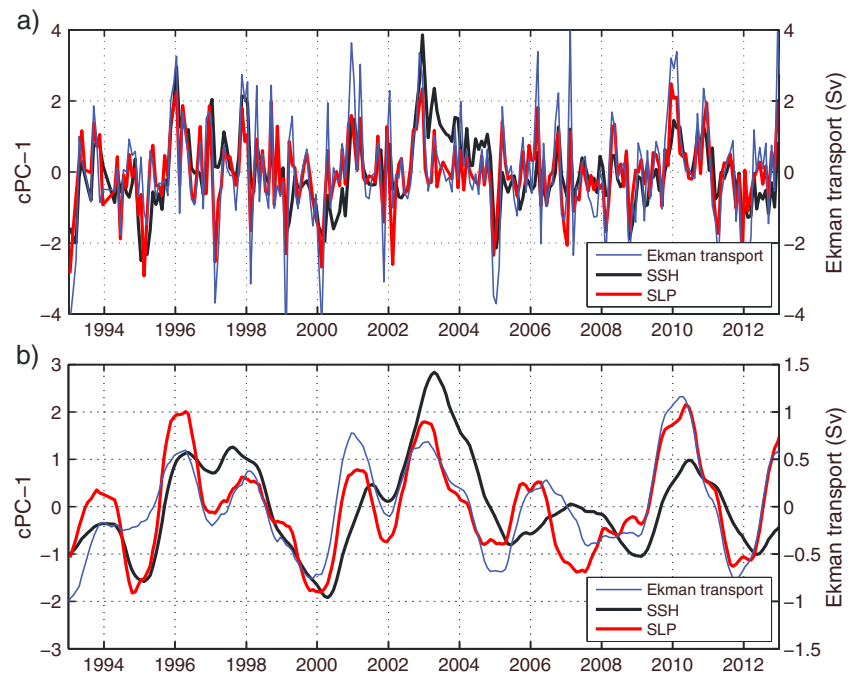


Figure 3. The cPC-1 of the (a) nonseasonal and (b) interannual SSH (black) and SLP (red). Blue curves show the nonseasonal and interannual time series of the net meridional Ekman transport at 60°N and between 40°W and 5°E.

3.2. Sea Level and Atmospheric Forcing

Coherent basin-wide changes of the nonseasonal OcM over the Arctic Ocean and the Nordic Seas and close agreement between the nonseasonal OcM and SSH in the Nordic and Barents Seas is a prerequisite for coupling satellite altimetry SSH to atmospheric forcing. Compared to the GRACE data, satellite altimetry provides a longer observational record and therefore gives more confidence in the statistical results.

The cEOF-1 mode exhibits covarying dipole oscillation patterns in both the SSH (Figure 2a) and SLP (Figure 2b) fields, with one center located in the Nordic Seas and the other over the midlatitude eastern North Atlantic. The cEOF-1 patterns for the nonseasonal and interannual fields are similar, and they explain 73% and 86% of the squared covariance, respectively. The values in homogeneous correlation maps over the Nordic Seas exceed 0.75 (Figure 2a and 2b) meaning that the cEOF-1 mode explains over 50% of the local SSH/SLP variance. The cPC-1 time series (Figure 3) demonstrate that both the short-period synoptic oscillations and the interannual changes of SSH and SLP are coherent. The maximum cross-correlation between the cPC-1 time series is 0.62 at zero lag for the nonseasonal fields (Figure 3a) and 0.72 with the cPC-1 of SSH lagging 3 months behind the cPC-1 of SLP for the interannual fields (Figure 3b). The cPC-1 time series of the interannual SSH and SLP show local maxima in 1996–1997, 2002–2003, 2006–2007, and 2010–2011, similar to Figure 1c.

These statistical results indicate that positive/negative SLP anomalies extending over a large area from Greenland to northern Europe are associated with positive/negative SSH anomalies over the Nordic Seas. This is expected, because the former drive anticyclonic/cyclonic wind anomalies that lead the Ekman convergence/divergence. The structure of wind anomaly vectors, associated with both the nonseasonal and interannual cPC-1 of SLP (Figure 2c), means that one standard deviation increase in cPC-1 of SLP over the Nordic Seas is associated with a local anticyclonic wind anomaly and with a much stronger zonal wind anomaly over the northeastern North Atlantic, centered at about 57°N.

Although the northward wind anomalies in the Greenland Sea are able to modify the strength of the East Greenland Current and the Ekman slope current across the Fram Strait [e.g., *Peralta-Ferriz et al.*, 2014; *Volkov and Landerer*, 2013], they seem to be insufficient to cause the observed basin-wide fluctuations of sea level and mass north of 65°N. The easterly/westerly wind anomalies over the northeastern North Atlantic south of

65°N appear to be much stronger (Figure 2c). These anomalies drive the northward/southward Ekman transport anomalies that can lead to an increase/decrease of SSH in the Nordic Seas and possibly over the entire Arctic Ocean. The net meridional Ekman transport at 60°N and between 40°W and 5°E correlates with both the cPC-1 of SLP and cPC-1 of SSH (Figure 3). The zero-lag correlation between the nonseasonal time series of the meridional Ekman transport and cPC-1 of SLP/SSH is 0.85/0.64. The maximum correlation between the interannual time series of the meridional Ekman transport and cPC-1 of SSH is 0.68 with the cPC-1 of SSH lagging 4 months behind.

Similar results, but for a shorter time interval (2003–2012), are obtained by coupling atmospheric forcing to the nonseasonal GRACE OCM (not shown). The zero-lag correlation between the nonseasonal time series of the Arctic OCM (averaged north of 65°N) and the net meridional Ekman transport at 60°N is small ($r = 0.19$), which means that the impact of additional processes, like wind-driven changes of circulation in the Nordic Seas and the Bering Strait transport [Volkov and Landerer, 2013; Peralta-Ferriz et al., 2014], is also important. On the other hand, the maximum correlation between the interannual time series is 0.65 with OCM lagging behind the Ekman transport by 9 months. The latter relationship supports the particular importance of the time integrated meridional Ekman transport in the northeast Atlantic on the interannual variability of the Arctic OCM. It should be noted that the near-surface Ekman dynamics are only half of the story because the net meridional Ekman transport is compensated by geostrophic return flows at depth.

The observed SLP and SSH variability pattern and the strength of the zonal winds in the northeastern North Atlantic are related to the North Atlantic Oscillation (NAO) [Hurrell, 2013]. The correlation between the cPC-1 of SLP and the monthly NAO index is -0.62 , while correlation between the cPC-1 of SSH and the monthly NAO index is -0.38 .

4. Conclusions

The GRACE satellites have observed coherent basin-wide changes of the nonseasonal OCM extending across the deep parts of the Arctic Ocean and the adjacent Nordic Seas. The existing explanation of the nonseasonal basin-wide OCM changes as being due only to the meridional wind anomalies over the Nordic Seas is not complete and an external forcing mechanism should also be relevant. The basin-wide coherency of the nonseasonal OCM variability and the strong correlation between the nonseasonal OCM and SSH over the Nordic and Barents Seas allows using the longer satellite altimetry records as a proxy for the nonseasonal SSH in the Arctic Ocean. Coupling the nonseasonal SSH variability to atmospheric forcing shows that positive/negative SLP anomalies are correlated with positive/negative SSH anomalies in the Nordic Seas. This is partly because of the associated local Ekman convergence/divergence. On the other hand, a dipole oscillation pattern of SLP drives strong zonal wind anomalies over the northeastern North Atlantic correlated with the nonseasonal SSH variability in the Nordic Seas. The variations of zonal wind cause the northward Ekman transport anomalies that modify the net transport across the boundary between the northeastern North Atlantic and the Nordic Seas. The results of this study demonstrate that the Ekman transport anomalies over the northeastern North Atlantic are very important for driving the nonseasonal, including interannual, variability of the Arctic OCM and SSH. This study complements previous research [Volkov and Landerer, 2013; Peralta-Ferriz et al., 2014] and extends it by using longer (compared to GRACE) satellite altimetry observations, identifying a new mechanism for the Arctic OCM/SSH variability, and establishing relationship between the interannual changes of the Arctic OCM/SSH and wind forcing.

References

- Bretherton, C. S., C. Smith, and J. M. Wallace (1992), An intercomparison of methods for finding coupled patterns in climate data, *J. Clim.*, *5*, 541–560.
- Chambers, D. P., and J. A. Bonin (2012), Evaluation of Release 05 time-variable gravity coefficients over the ocean, *Ocean Sci.*, *8*, 859–868, doi:10.5194/os-8-859-2012.
- Dee, D. P., et al. (2011), The ERA-Interim reanalysis: Configuration and performance of the data assimilation system, *Q. J. R. Meteorol. Soc.*, John Wiley & Sons, Ltd., *137*, 553–597.
- Hurrell, J. (2013), The climate data guide: Hurrell North Atlantic Oscillation (NAO) Index (PC-based) retrieved from <https://climatedataguide.ucar.edu/guidance/hurrell-north-atlantic-oscillation-nao-index-pc-based>, Tech. rep., NCAR, Boulder, Colo.
- Kwok, R., and J. Morison (2011), Dynamic topography of the ice-covered Arctic Ocean from ICESat, *Geophys. Res. Lett.*, *38*, L02501, doi:10.1029/2010GL046063.
- Le Traon, P.-Y., F. Nadal, and N. Ducet (1998), An improved mapping method of multisatellite altimeter data, *J. Atmos. Oceanic Technol.*, *15*, 522–534.

Acknowledgments

The GRACE ocean data were processed by Don P. Chambers, supported by the NASA MEASURES Program (<http://grace.jpl.nasa.gov>). The SSH data were produced by Ssalto/Duacs and distributed by Aviso (www.aviso.oceanobs.com) with support from CNES. This research was funded by the NASA Physical Oceanography program (grant NNX11AE27G) and carried out at the NOAA Atlantic Oceanographic and Meteorological Laboratory. The author thanks Sang-Ki Lee, Elizabeth Johns, Cecilia Peralta-Ferriz, the Editor, and an anonymous reviewer for reviewing the paper and providing their comments and suggestions.

The Editor thanks Don Chambers and an anonymous reviewer for their assistance evaluating this manuscript.

- Morison, J., J. Wahr, R. Kwok, and C. Peralta-Ferriz (2007), Recent trends in Arctic Ocean mass distribution revealed by GRACE, *Geophys. Res. Lett.*, *34*, L07602, doi:10.1029/2006GL029016.
- Peacock, N. R., and S. W. Laxon (2004), Sea surface height determination in the Arctic Ocean from ERS altimetry, *J. Geophys. Res.*, *109*, C07001, doi:10.1029/2001JC001026.
- Peralta-Ferriz, C., and J. Morison (2010), Understanding the annual cycle of the Arctic Ocean bottom pressure, *Geophys. Res. Lett.*, *37*, L10603, doi:10.1029/2010GL042827.
- Peralta-Ferriz, C., J. H. Morison, J. M. Wallace, and J. Zhang (2011), A basin-coherent mode of sub-monthly variability in the Arctic Ocean, *Geophys. Res. Lett.*, *38*, L14606, doi:10.1029/2011GL048142.
- Peralta-Ferriz, C., J. H. Morison, J. M. Wallace, J. A. Bonin, and J. Zhang (2014), Arctic Ocean circulation patterns revealed by GRACE, *J. Clim.*, *27*, 1445–1468, doi:10.1175/JCLI-D-13-00013.1.
- Ponte, R. M., K. J. Quinn, C. Wunsch, and P. Heimbach (2007), A comparison of model and GRACE estimates of the large-scale seasonal cycle in ocean bottom pressure, *Geophys. Res. Lett.*, *34*, L09603, doi:10.1029/2007GL029599.
- von Storch, H., and F. W. Zwiers (1999), *Statistical Analysis in Climate Research*, Cambridge Univ. Press, Cambridge, U. K.
- Tapley, B. D., S. Bettadpur, J. R. Ries, P. F. Thompson, and M. M. Watkins (2004), GRACE measurements of mass variability in the Earth systems, *Science*, *305*, 503–505.
- Vinogradova, N. T., R. M. Ponte, and D. Stammer (2007), Relation between sea level and bottom pressure and the vertical dependence of oceanic variability, *Geophys. Res. Lett.*, *34*, L03608, doi:10.1029/2006GL028588.
- Volkov, D. L., and F. W. Landerer (2013), Nonseasonal fluctuations of the Arctic Ocean mass observed by the GRACE satellites, *J. Geophys. Res. Oceans*, *118*, 6451–6460, doi:10.1002/2013JC009341.
- Volkov, D. L., and M.-I. Pujol (2012), Quality assessment of a satellite altimetry data product in the Nordic, Barents, and Kara Seas, *J. Geophys. Res.*, *117*, C03025, doi:10.1029/2011JC007557.
- Volkov, D. L., F. W. Landerer, and S. A. Kirillov (2013), The genesis of sea level variability in the Barents Sea, *Cont. Shelf Res.*, *66*, 92–104, doi:10.1016/j.csr.2013.07.007.